

Prediction Model of Aircraft Icing Based on Deep Neural Network

YI Xian^{1,2,3*}, WANG Qiang^{1,2,3*}, CHAI Congcong^{1,4}, GUO Lei⁴

1. Low Speed Aerodynamic Institute, China Aerodynamics Research and Development Center (CARD C),
Mianyang 610082, P. R. China;

2. Anti/de-icing Key Laboratory, China Aerodynamics Research and Development Center (CARD C),
Mianyang 610082, P. R. China;

3. State Key Laboratory of Aerodynamics, Mianyang 610082, P. R. China;

4. School of Computer Science and Engineering, University of Electronic Science and Technology of China,
Chengdu 610000, P. R. China

(Received 10 June 2021; revised 20 July 2021; accepted 8 August 2021)

Abstract: Icing is an important factor threatening aircraft flight safety. According to the requirements of airworthiness regulations, aircraft icing safety assessment is needed to be carried out based on the ice shapes formed under different icing conditions. Due to the complexity of the icing process, the rapid assessment of ice shape remains an important challenge. In this paper, an efficient prediction model of aircraft icing is established based on the deep belief network (DBN) and the stacked auto-encoder (SAE), which are all deep neural networks. The detailed network structures are designed and then the networks are trained according to the samples obtained by the icing numerical computation. After that the model is applied on the ice shape evaluation of NACA0012 airfoil. The results show that the model can accurately capture the nonlinear behavior of aircraft icing and thus make an excellent ice shape prediction. The model provides an important tool for aircraft icing analysis.

Key words: aircraft icing; ice shape prediction; deep neural network; deep belief network; stacked auto-encoder

CLC number: O359 **Document code:** A **Article ID:** 1005-1120(2021)04-0535-10

0 Introduction

Icing is a widespread physical phenomenon in the actual flight of aircraft leading to safety accidents. During aircraft passing through the clouds, the supercooled water droplets in the air can impinge on the surface of the aircraft.

When the ambient temperature and the liquid water content (LWC) are relatively low, the water droplets may freeze immediately. As a result, the opaque and milky white rime ice is usually generated. In contrast, at a relative higher temperature and LWC condition, a part of the water droplets may not freeze on impact and the remaining liquid water will form a water film, move on the surface of the aircraft driven by the wind shear stress force, the surface tension force, the gravity force, etc., and

gradually freeze during the movement. At this condition, the clear transparent glaze ice or the mixed ice will be formed^[1].

The ice accretion may pose a great threat to the aircraft safety. On one hand, accreted ice can greatly change the aerodynamic shape of the lifting surface of the aircraft, and lead to the decrease of the lift force and the increase of the drag force. On the other hand, the icing on the control surface will result in a significant reduction in aircraft handling performance^[2]. In addition, the irregular ice shedding is also a great threat to the engine and other components^[3].

In order to effectively reduce the risk of icing accidents, different airworthiness regulations have been issued by Federal Aviation Administration (FAA) and other management^[4-5], in which a com-

*Corresponding authors, E-mail addresses: yixian@cardc.cn; wangqiang@cardc.cn.

How to cite this article: YI Xian, WANG Qiang, CHAI Congcong, et al. Prediction model of aircraft icing based on deep neural network[J]. Transactions of Nanjing University of Aeronautics and Astronautics, 2021, 38(4):535-544.

<http://dx.doi.org/10.16356/j.1005-1120.2021.04.001>

prehensive assessment of flight safety under icing condition is required. To accurately analyze the influence of ice accretion, lots of ice shapes are needed to be evaluated. So far the acquisition of ice shape mainly relies on icing wind tunnel experiments and numerical calculations. Generally, the icing wind tunnel test is so expensive that only limited icing conditions can be performed. Therefore, the wind tunnel test is usually conducted to demonstrate the critical ice shape^[6] and before that a lot of icing numerical computations are carried out.

Recently, the icing numerical calculation methods have been developed rapidly, but it is still time consuming since the accurate ice shape simulation requires the cyclic iteration of the flow field calculation, the water collection computation, the water-to-ice phase change analysis and the grid deformation^[7]. Therefore, how to improve the computation efficiency has always been the goal of icing research.

The artificial neural networks (ANNs) provide a new way to solve the problem. In recent years, with the continuous updating of the structure and learning algorithm of the neural network, its strong learning capability and good fault tolerance provide a powerful tool for the rapid prediction of aircraft ice shape. Ogretim et al.^[8] believed that although the icing phenomenon contains complex nonlinear characteristics, the nonlinear system representation capability of neural network can be used to simulate the physical process of icing. For this reason, they developed a rime ice prediction network based on the general regression neural network (GRNN) and a glaze ice prediction network based on the back-propagation network (BP) by using the Fourier transform of airfoil surface ice shape^[8]. In order to improve the description accuracy of the complex ice shape, Chang et al.^[9] proposed a combined ANN ice prediction method based on discrete wavelet transform. They demonstrated that the GRNN network can achieve better performance than the BP network and the radial basis function (RBF) network^[9]. However, the current ice prediction ANNs are mainly based on shallow neural network models, which may be unable to learn the extremely complex icing process.

By contrast, the deep neural network (DNN) can represent more complex nonlinear physical phenomena through a large number of hidden layer network structures, which is believed to make a better prediction of complex ice shapes. However, although DNN has been applied in different fields^[10-12], this method has not been widely used in the field of icing research.

In this paper, the airfoil ice shape prediction model based on DNN is established, in which the deep belief network (DBN) and the stacked auto-encoder (SAE) are utilized to simulate the ice thickness distribution along the airfoil surface and the ice shape characteristic parameters. The detailed structure of the deep neural networks is determined by error analysis caused by the number of the hidden layers and neurons. The coupled unsupervised and supervised training strategy is applied, which effectively promotes the network training process. The results demonstrate that DNNs are capable of describing the complex nonlinear relationship involved in the ice shape prediction and thus predicting the ice shapes more accurately than BP network. The model can be used to analyze the flight safety of aircraft in complex ice environment.

1 Ice Shape Sample Set

1.1 Ice shape numerical computation

A CFD-based icing computational model is applied for the ice shape computation. The single step computation method is utilized in the computation, so there are three modules involved in the model, including the flow field calculation, the water collection analyzation, and the ice phase change simulation.

1.1.1 Flow field calculation module

The flow field is computed by the finite volume method (FVM) and the incompressible Navier-Stokes equations are solved by the semi-implicit method for pressure linked equations (SIMPLEs). The control equation can be written as

$$\frac{\partial \rho \phi}{\partial t} + \nabla \cdot (\rho \mathbf{v} \phi - \Gamma_{\phi} \nabla \phi) = q_{\phi} \quad (1)$$

where ϕ denotes the variables to be solved, ρ the den-

sity of the fluid, \mathbf{v} the velocity vector, Γ_ϕ the corresponding diffusion coefficient and q the source item. The detailed information can be found in Ref. [13].

1.1.2 Water collection calculation module

By tracking the trajectories of water droplets, the Lagrangian method is efficient in 2D water collection computation, which is utilized to find out collected liquid water impinged on the surface of airfoil. Eqs.(2,3) are the kinematic equations of water droplet motion.

$$\frac{d\mathbf{u}_d}{dt} = \frac{(\rho_d - \rho_a)}{\rho_d} g + \frac{C_d \cdot Re_d}{24} \cdot \frac{18\mu_a}{\rho_d \cdot D^2} (\mathbf{u}_a - \mathbf{u}_d) \quad (2)$$

$$\frac{C_d \cdot Re_d}{24} = 1.0 + 0.197Re_d^{0.63} + 2.6 \times 10^{-4} Re_d^{1.38} \quad (3)$$

where \mathbf{u}_d is the droplet velocity, t the time, g the gravity acceleration, C_d the drag coefficient, Re_d the relative Reynolds number, and D the diameter of the droplet. ρ_d and ρ_a are the densities of the water droplet and air, respectively. The water collection calculation module has been validated by comparison of the computed collection efficiency of the 30P30N multi-segment wing model with the experimental data at different conditions of the angle of attack (AOA) and the median volume diameter (MVD), as shown in Fig.1.

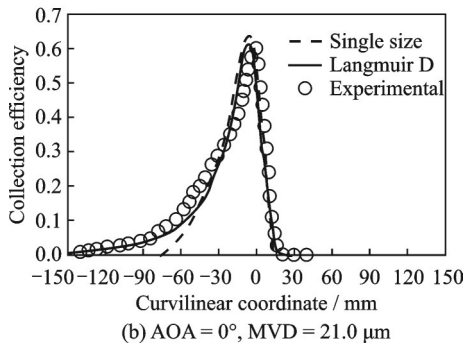
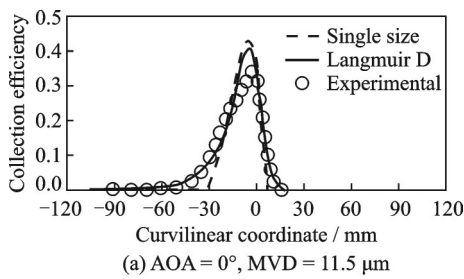


Fig.1 Water collection efficiency comparison between computed result and experimental data at different conditions

1.1.3 Phase change calculation module

Once the collected water is obtained, the classic Messinger model^[14] is used to simulate the ice phase change process on the airfoil to simulate the ice growth process. The basic mass and energy conservation equations are solved in the module as shown in Eqs.(4,5).

$$\dot{m}_{imp} + \dot{m}_{in} = \dot{m}_{sol} + \dot{m}_{evp} + \dot{m}_{out} \quad (4)$$

$$\dot{Q}_{imp} + \dot{Q}_{in} + \dot{Q}_{sol} = \dot{Q}_{con} + \dot{Q}_{evp} + \dot{Q}_{out} \quad (5)$$

where \dot{m}_{imp} is the impinged liquid water, \dot{m}_{in} the flow coming from the previous computational element, and \dot{m}_{out} the water flowing into the next computational element. \dot{m}_{sol} and \dot{m}_{evp} are the frozen and evaporated liquid water. The corresponding energy items are shown in Eq.(5). For more information, please refer to Ref. [14].

To validate the model, the icing wind tunnel experimental data are used, which are cut at the wing tip of a certain aircraft. The experiment is carried in the 3 m×2 m icing wind tunnel of China Aerodynamics Research and Development Center. Fig.2 shows the ice shape comparison between the computational results and the icing wind tunnel results at different conditions of wind speed V , static temperature T_s , MVD, liquid water content

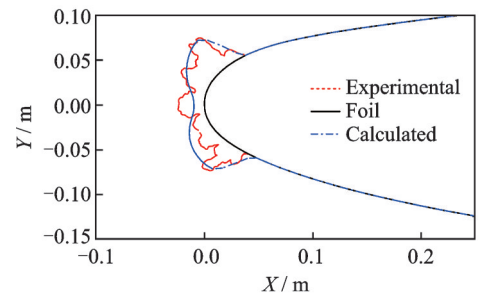
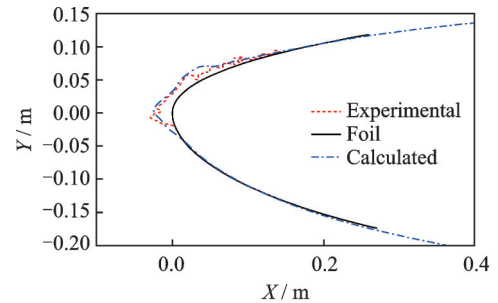


Fig.2 Ice shape comparison between the computed result and experimental data at different conditions

(LWC), altitude H and time. It can be seen that in both of the rime ice and glaze ice conditions, the calculated ice shapes agree well with the experimental data.

1.2 Fourier transform of the ice shape curve

The description of the ice shape determines the output dimension of the DNN. The smaller output dimension will greatly simplify the simulation difficulty of the DNN. In this paper, the Fourier transform method, as proposed in Ref.[8], is used to describe the ice shape, shown as

$$\tilde{T}(\xi) = \frac{a_0}{2} + \sum_{i=1}^n \left[a_i \cos\left(\frac{2\pi i \xi}{\xi_u - \xi_l}\right) + b_i \sin\left(\frac{2\pi i \xi}{\xi_u - \xi_l}\right) \right] \quad (6)$$

$$a_i = \frac{2}{\xi_u - \xi_l} \int_{\xi_l}^{\xi_u} T(\xi) \cos\left(\frac{2\pi i \xi}{\xi_u - \xi_l}\right) d\xi \quad i = 1, 2, \dots, n \quad (7)$$

$$b_i = \frac{2}{\xi_u - \xi_l} \int_{\xi_l}^{\xi_u} T(\xi) \sin\left(\frac{2\pi i \xi}{\xi_u - \xi_l}\right) d\xi \quad i = 1, 2, \dots, n \quad (8)$$

where \tilde{T} is the curve of ice thickness in curvilinear coordinates and ξ the wall curvilinear coordinate. a_i and b_i are the Fourier coefficients, and ξ_l and ξ_u the ice accretion limits on the lower and upper surfaces of the airfoil. And n is the number of the expansion items, which is assumed to be 30 in this paper.

1.3 Ice shape characteristic parameters

In order to further reduce the degrees of the ice shape representation, eight ice shape characteristic parameters proposed in SAE standard^[15] are used.

As shown in Fig.3, the eight ice shape characters are the upper horn peak thickness h_u , the lower horn peak thickness h_l , the upper horn angle θ_u , the

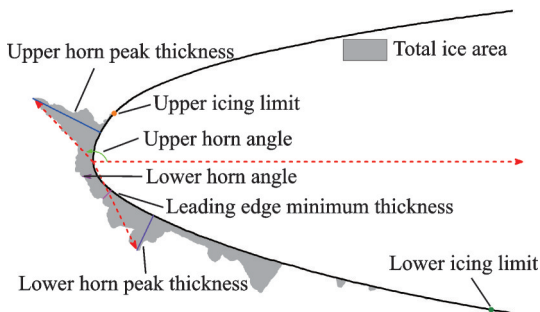


Fig.3 Ice shape parameters defined in the SAE standard^[15]

lower horn angle θ_l , the upper icing limit ξ_u , the lower icing limit ξ_l , the leading edge minimum thickness h_{sp} , and the total ice area S_{ice} .

The ice shape Fourier coefficients and the eight parameters are two different ways of describing ice shape. Both of them will be designed as the output of the DNN in this paper.

1.4 Ice shape sample set

Based on the established computational method, the following icing environmental parameters will be considered in NACA0012 airfoil icing computation. The detailed information is shown in Table 1.

Table 1 Range of icing environmental parameters in the sample set

Parameter	Parameter range
$V/(m \cdot s^{-1})$	60—150
Temperature T/K	243—268
LWC/ $(g \cdot m^{-3})$	0.1—1.25
MVD/ μm	15—60
Icing time t/s	300—2 700

A total of 11 258 ice shape samples are obtained. Each sample is composed of three parts: (1) Five input icing parameters (V , T , LWC, MVD, t); (2) 31 Fourier coefficients a_i and 30 Fourier coefficients b_i ; (3) eight ice shape characteristic parameters $h_u, h_l, \theta_u, \theta_l, \xi_u, \xi_l, h_{sp}, S_{ice}$.

2 DNN for Ice Shape Prediction

2.1 Deep belief network

DBN is a probabilistic generation model, and usually composed of several restricted Boltzmann machines (RBMs)^[16]. Generally, each RBM has two layers. The first one is called the visible layer or input layer, and the second one is called the hidden layer. The layers are fully connected with each other, but the neurons in the layers are not connected. In current study, an additional BP layer is involved which outputs the final ice shape information. The structure of the DBN is shown in Fig.4.

The training process of the DBN can be divided into two parts: The unsupervised pre-training of RBM and the supervised reverse parameter adjust-

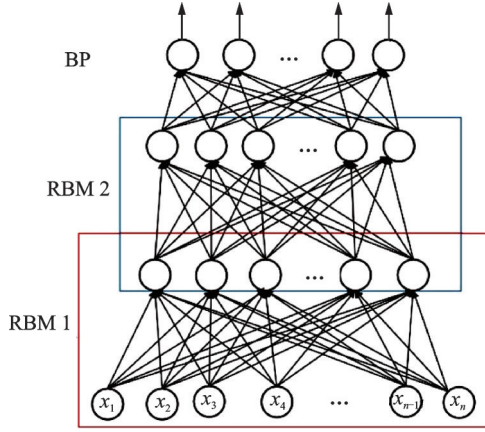


Fig.4 DBN network structure

ment. The CD- k algorithm ($k=1$) and the Gibbs sampling^[17] are used in the pre-training stage to update the weight and deviation of RBM. The detailed training process includes the following steps.

2.1.1 RBM initialization

The RBM is needed to be initialized before training the network as

$$\left\{ \begin{array}{l} \mathbf{W}^i = \begin{bmatrix} W_{1,1}^i & W_{2,1}^i & \cdots & W_{V,1}^i \\ W_{1,2}^i & W_{2,2}^i & \cdots & W_{V,2}^i \\ \vdots & \vdots & \ddots & \vdots \\ W_{1,H}^i & W_{2,H}^i & \cdots & W_{V,H}^i \end{bmatrix} \\ \mathbf{v}_b^i = \begin{bmatrix} v_{b1}^i \\ v_{b2}^i \\ \vdots \\ v_{bV}^i \end{bmatrix}, \mathbf{h}_b^i = \begin{bmatrix} h_{b1}^i \\ h_{b2}^i \\ \vdots \\ h_{bH}^i \end{bmatrix} \end{array} \right. \quad i=0, 1, \dots, N-1 \quad (9)$$

where N is the number of RBM and \mathbf{W}^i the weight of the i th RBM. \mathbf{v}_b^i and \mathbf{h}_b^i are the offset vectors of the visible and hidden layers respectively. \mathbf{W}^i is initialized by the Xavier method to make the weight uniformly distribute in the following interval, shown as

$$\mathbf{W}^i \in U \left[-\sqrt{\frac{6}{n^l + n^{l+1}}}, \sqrt{\frac{6}{n^l + n^{l+1}}} \right] \quad l=0, 1, \dots, L-1 \quad (10)$$

where U is the uniform distribution, L the number of hidden layers, and n^l the number of the neural in the l th hiding layer. All the offset vectors are set as zero.

2.1.2 Weight and deviation update

The training is carried out layer-by-layer. Firstly, suppose \mathbf{v}^0 equals to the input vector \mathbf{X} . Then, the forward training was carried out to calculate the probability of hidden layer neurons of RBM, and

the activation vector of hidden layer was obtained by Gibbs sampling from this probability distribution, shown as

$$\mathbf{h}^0 = \text{Gibbs_sampleProb} [\sigma(\mathbf{v}^0 \otimes \mathbf{W}^0 + \mathbf{h}_b^0)] \quad (11)$$

$$\sigma(x) = \frac{1}{1 + e^{-x}} \quad (12)$$

where σ is the activation function. In this paper the Sigmoid function is taken as the activation function.

The positive forward gradient can be calculated as

$$\text{grad_pos} = \mathbf{v}^0 \otimes \mathbf{h}^0 \quad (13)$$

Thirdly, based on \mathbf{h}^0 , \mathbf{v}^0 is reconstructed as

$$\tilde{\mathbf{v}}^0 = \text{Gibbs_samplePro} [\sigma(\mathbf{h}^0 \otimes (\mathbf{W}^0)^T + \mathbf{v}_b^0)] \quad (14)$$

and \mathbf{h}^0 can be also updated as

$$\tilde{\mathbf{h}}^0 = \sigma(\tilde{\mathbf{v}}^0 \otimes \mathbf{W}^0 + \mathbf{h}_b^0) \quad (15)$$

Thus the negative forward gradient can be written as

$$\text{grad_neg} = \tilde{\mathbf{v}}^0 \otimes \tilde{\mathbf{h}}^0 \quad (16)$$

Finally, the weight and deviation of RBM can be updated by Eqs.(17–20).

$$\text{CD} = \frac{\text{grad_pos} - \text{grad_neg}}{n^0} \quad (17)$$

$$\tilde{\mathbf{W}}^0 = \mathbf{W}^0 + \alpha \cdot \text{CD} \quad (18)$$

$$\tilde{\mathbf{v}}_b^0 = \mathbf{v}_b^0 + \alpha \cdot \text{mean}(\mathbf{v}^0 - \tilde{\mathbf{v}}^0) \quad (19)$$

$$\tilde{\mathbf{h}}_b^0 = \mathbf{h}_b^0 + \alpha \cdot \text{mean}(\mathbf{h}^0 - \tilde{\mathbf{h}}^0) \quad (20)$$

where $\text{mean}(\cdot)$ refers to calculate average value.

The computation is carried out iteratively until the error reaches the threshold or the number of iterations reaches the limit.

2.1.3 Supervised reverse tuning parameters

Reverse adjustment parameters with supervision include weight deviation initialization, forward error propagation and back propagation of the BP layer. The weight deviation initialization of the BP layer is the same as that of the RBM layer. In forward propagation, the output value calculated by the connected DBN is transferred forward, while the back propagation uses the BP algorithm for iterative training. The whole training process stops until the error function reaches the setting value or the number of training reaches the limit.

2.2 Stacked auto-encoder

The SAE is also a kind of deep neural network consisting of a stack of auto-encoder (AE) units to

perform the task of layer-by-layer feature extraction. Generally speaking, one AE can be divided into two parts: Encoder input and decoder. As shown in Fig.5, the SAE network has a similar structure to DBN, which has a layer of the BP network at the end.

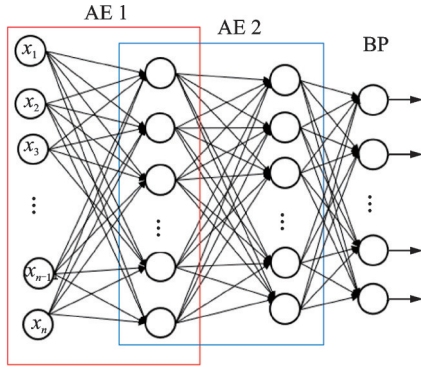


Fig.5 SAE network structure

The training process of the SAE network is similar to that of DBN, mainly including unsupervised pre-training and supervised fine-tuning of AE. The unsupervised pre-training process of AE includes the following steps.

Firstly, the encoder transfers the input vector x from the input layer to the hidden layer through the activation function σ .

$$h = \sigma(Wx + b) \quad (21)$$

Secondly, the decoder maps the hidden layer h to the output layer to reconstruct the input vector through the activation function σ .

$$\tilde{x} = \sigma(\tilde{W}h + \tilde{b}) \quad (22)$$

Then the reconstruction error is defined as

$$J(W, \tilde{W}, h, \tilde{h}) = \sum_{i=1}^N \|\tilde{x}_i - x_i\|^2 \quad (23)$$

The weights and deviations of SAE are constantly updated by the minimization of the reconstruction error.

In this paper, the maximum number of iterations of network training is set as 50 000 times and the learning rate is taken as $1E-5$. The loss function adopts mean square error (MSE), which is defined as

$$\text{MSE} = \frac{\sum_{i=1}^n (\tilde{y}_i - y_i)^2}{n} \quad (24)$$

where y_i is the original data, \tilde{y}_i the prediction data and n the number of the samples.

3 Results and Analysis

3.1 Error analysis

The number of neurons and hidden layers are important parameters for DNN, which not only determines the generalization performance but also influences the training process. Too many neurons will lead to over-fitting and too long training time. In contrast, if the number of neurons is too small, it will lead to under-fitting and the physical law cannot be captured by network.

In order to analyze the error caused by the number of neurons and hidden layers in different DNNs. Different conditions are considered in DBN and SAE, as shown in Table 2.

Table 2 Different DNN structures considered in the model

Ice shape description parameter	Number of neurons	Number of hidden layers
a_i	7, 11, 15, 20, 50	2, 4, 6, 8
b_i	7, 11, 15, 20, 50	2, 4, 6, 8
Ice shape characteristic parameters	5, 6, 8, 10, 15	2, 3, 4, 6

Both of the DBN and SAE networks are applied in prediction of the ice shape curve and the eight parameters. The best performance network is summarized in Table 3.

From Table 3, it can be seen that the minimum MSE of a_i and b_i is obtained by the SAE network. But for ice shape characteristic parameter prediction, the DBN network is more accurate. As a result, in the following analysis, the SAE network with 2 hidden layers/20 neurons and 4 hidden layers/15 neurons will be used in prediction of a_i and b_i , respectively. At the same time, the DBN network with 6 hidden layers/8 neurons will be applied

Table 3 The best performance DNN in ice shape and characteristic parameter prediction

Network structure	a_i	b_i	Eight ice shape characteristic parameter
Layer	2(SAE)	4(SAE)	6(DBN)
Neuron	20(SAE)	15(SAE)	8(DBN)
MSE	0.044	0.031	0.006

in the eight ice shape characteristic parameter prediction.

3.2 Ice shape curve prediction based on SAE

In order to demonstrate the accuracy of the established SAE network, the following icing environment conditions will be tested. The detailed information is shown in Table 4.

Table 4 Icing conditions for analysis of SAE network

Case No.	V/ (m•s ⁻¹)	T/K	LWC/ (g•m ⁻³)	MVD/ μm	t/s
1	150	243	0.4	60	1 350
2	110	253	1.0	35	600
3	70	254	1.0	34	602
4	128	242	1.26	16	1 005

The prediction results are shown in Fig.6. As a comparison, the prediction results of the BP network are also included. From the comparison, it can be seen that the ice shape predicted by SAE is extremely close to the icing numerical results for both of the Rime Ice condition (Case No.1) and the Glaze/Mixed Ice conditions (Case Nos.2—4). The predicted ice accreted area and the ice horns are highly consistent with the numerical calculated data. Besides, by comparing the BP results, we can see that the deep neuron network can make a better prediction of the ice shape especially for the Glaze/Mixed Ice conditions when the ice shape is extremely complex and the nonlinear behavior is dominated.

In order to quantitatively evaluate the accuracy of the model, the following ice shape consistency index Par is utilized, which is proposed in Ref. [18].

$$Par = 0.7(1 - Dia) + 0.3(1 - Rat) \quad (25)$$

where Dia is the ice shape geometric characteristic similar parameter, shown as

$$Dia = \sum_{i=1}^n \left| \frac{\tilde{x}_i - x_i}{x_i} \right| \times 100\% \quad (26)$$

where \tilde{x}_i and x_i are discrete points of the predicted and target ice shapes.

And Rat is the ice shape difference rate parameter, which is defined as

$$Rat = \frac{S_{diff}}{S_{ave}} \quad (27)$$

where S_{diff} is the difference of the ice shape and S_{ave}

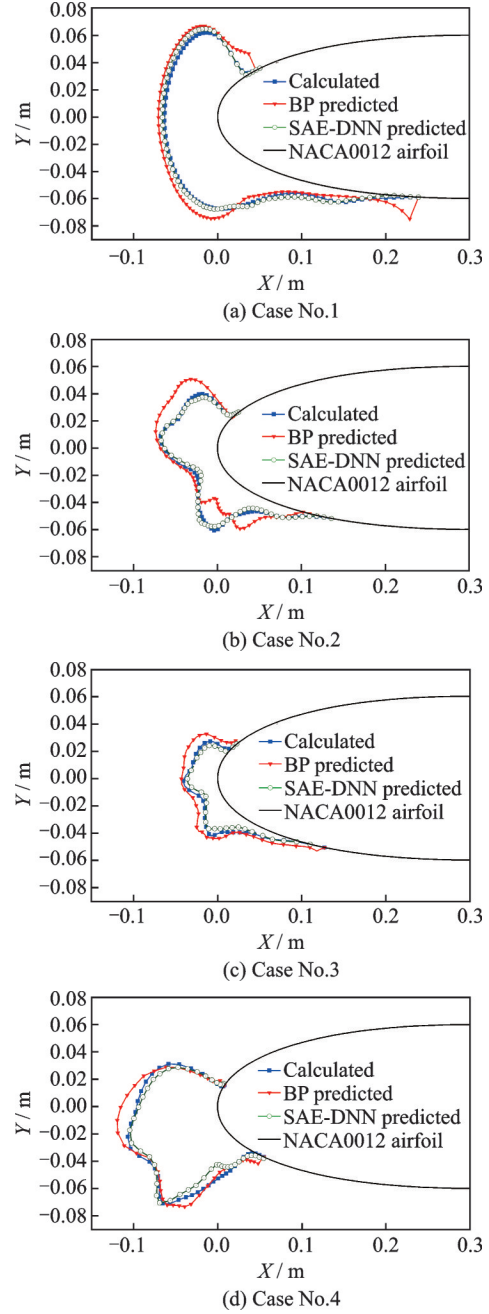


Fig.6 Comparison of ice shape among SAE and BP predictions and icing numerical computation

the averaged value of ice shape.

According to the ice shapes predicted by SAE and BP, the corresponding ice shape consistency indexes are compared in Table 5. For all the four cas-

Table 5 Comparison of ice shape consistency indexes %

Case No.	SAE	BP
1	97.19	90.48
2	95.38	86.91
3	92.04	87.50
4	93.05	90.20

es, the consistency indexes predicted by SAE are higher than 90%. Especially for the Rime Ice condition (Case No.1), the consistency index of SAE is as high as 97.19%. By contrast, the ice shape predicted by the BP network is less accuracy. For Glaze/Mixed Ice condition (Case No.2), the BP network can predict the ice shape with only 86.91% accuracy.

In addition, to further validate the capability of the SAE network, two icing wind tunnel experimental cases of NACA0012 airfoil^[19] are considered, as shown in Table 6.

Table 6 Experimental conditions for analysis of SAE network

Case No.	$V/(\text{m}\cdot\text{s}^{-1})$	T/K	$\text{LWC}/(\text{g}\cdot\text{m}^{-3})$	$\text{MVD}/\mu\text{m}$	t/s
5	102.8	256.49	0.55	20	420
6	102.8	262.04	1.3	30	360

Fig.7 shows the ice shape curve comparison between the predicted results and the experimental data. From Fig.7, it can see that the predicted results of SAE are close to the experimental data, which demonstrate that the SAE network has excellent generalization capability.

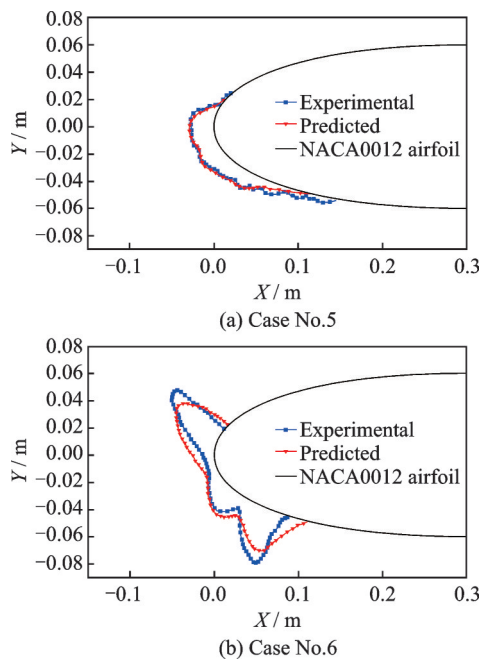


Fig.7 Comparison of ice shape between the SAE prediction and the icing wind tunnel experimental results

3.3 Ice shape characteristic parameter prediction based on DBN

In this section, the ice shape characteristic parameter prediction based on DBN will be discussed. The main characteristic parameter prediction errors of DBN are compared with those of BP network, as shown in Table 7.

From Table 7, it can be seen that the ice shape characteristic parameters predicted by DBN network are more accurate than those of BP network for all the four cases. In particular, for the Case No.1 and Case No.2, the prediction accuracy of DBN network is one order of magnitude higher than that of BP network. In Glaze/Mixed Ice conditions (Case Nos.3—4), although the prediction results of the two networks are close for some parameters, DBN network performs better in most of the conditions. These data quantitatively prove that, due to more hidden layers involved, the nonlinear representation capability of deep neuron network is enhanced. Thus the complex nonlinear behavior during the ice accretion can be better captured by the deep neuron network.

Table 7 Error comparison of ice shape characteristic parameters

Case No.	Model	S_{ice}	h_{sp}	h_{u}	h_{l}	θ_{u}	θ_{l}
1	DBN	0.43	3.23	0.00	1.61	0.96	0.42
	BP	10.29	11.29	12.70	11.29	3.73	1.08
2	DBN	0.57	6.90	1.47	0.00	0.29	0.50
	BP	7.95	17.24	8.82	17.78	1.04	1.73
3	DBN	0.57	6.90	1.47	0.00	0.29	0.50
	BP	10.63	42.86	4.88	22.58	1.20	1.60
4	DBN	5.80	4.71	1.83	3.26	0.52	0.72
	BP	3.77	3.53	10.09	2.17	1.25	1.07

4 Conclusions

The safety assessment of aircraft icing is strongly dependent on the rapid and accurate ice shape prediction method. The deep neuron network provides a new solution for aircraft ice shape analysis. In this paper, an accurate and efficient airfoil ice shape prediction model based on the DBN and SAE deep neuron networks are proposed, in which multi-

ple hidden layers are involved to capture the complex ice accretion process. According to the ice shape data set of NACA0012 airfoil computed by the CFD-based icing numerical computation, the DBN and SAE deep neuron networks are trained and the network structure as well as the corresponding prediction capabilities are analyzed.

The results show that: (1) The established model can make a good prediction of the ice shape and the ice shape characteristic parameters; (2) compared with the traditional shallow neural network models, such as BP, the deep neuron networks have great advantages in describing the complex nonlinear relationship of ice accretion; (3) the error analysis demonstrates that the SAE network can make a more accurate prediction of the ice shape curve, while the DBN network is more suitable for ice shape characteristic parameter prediction. The proposed model can be used as an effective tool in the aircraft icing safety assessment.

References

- [1] GENT R W, DART N P, CANSDALE J T. Aircraft icing[J]. *Philos Trans R Soc London A Math Phys Eng Sci*, 2000 (358): 2873-2911.
- [2] COLE J, SAND W. Statistical study of aircraft icing accidents[C]//*Proceedings of the 29th Aerospace Sciences Meeting*. [S.l.]: AIAA, 1991: 558.
- [3] VENKATARAMANI K, PLYBON R, HOLM R, et al. Aircraft engine icing model[C]//*Proceedings of the 46th AIAA Aerospace Sciences Meeting and Exhibit*. [S.l.]: AIAA, 2008: 440.
- [4] Federal Aviation Administration. Certification of transport category airplanes for flight in icing conditions: FAA AC25.1419-1A[S]. USA: Federal Aviation Administration, 2004.
- [5] Civil Aviation Administration of China. CCAR25 transport category aircraft certification standards[S]. China: Civil Aviation Administration of China, 2011.
- [6] DAVID C P. Developing critical ice shapes for use in aircraft development and certification: AIAA-2007-91 [R].[S.l.]: AIAA, 2007.
- [7] ALIAGA C N, AUBÉ M S, BARUZZI G S, et al. FENSAP-ICE-Unsteady: Unified in-flight icing simulation methodology for aircraft, rotorcraft, and jet engines[J]. *Journal of Aircraft*, 2011, 48(1): 119-126.
- [8] OGRETIM E, HUEBSCH W, SHINN A. Aircraft ice accretion prediction based on neural networks[J]. *Journal of Aircraft*, 2006, 43(1): 233-240.
- [9] CHANG Shinan, LENG Mengyao, WU Hongwei, et al. Aircraft ice accretion prediction using neural network and wavelet packet transform[J]. *Aircraft Engineering and Aerospace Technology*, 2016, 88 (1) : 128 -136.
- [10] DOWDEN B, DE SILVA O, HUANG W, et al. Sea ice classification via deep neural network semantic segmentation[J]. *IEEE Sensors Journal*, 2020. DOI: 10.1109/JSEN.2020.3031475.
- [11] CHEN Longting, XU Guanghua, LIANG Lin, et al. Learning deep representation for blades icing fault detection of wind turbines[C]//*Proceedings of 2018 IEEE International Conference on Prognostics and Health Management (ICPHM)*. [S.l.]: IEEE, 2018.
- [12] KRETUZ M, AIT-ALLAC A, VARASTEK K, et al. Machine learning-based icing prediction on wind turbines[C]//*Proceedings of the 52nd CIRP Conference on Manufacturing Systems*. Ljubljana, Slovenia: [s. n.], 2019: 423-428.
- [13] YI Xian, GUI Yewei, ZHU Guolin. Numerical method of a three-dimensional ice accretion model of aircraft[J]. *Acta Aeronautica et Astronautica Sinica*, 2010(11): 2151-2158. (in Chinese)
- [14] WANG Q, YI X. Simulation and analysis of wind turbine ice accretion under yaw condition via an improved multi-shot icing computational model[J]. *Renewable Energy*, 2020, 162: 1854-1873.
- [15] SAE International Group. Icing wind tunnel interfacility comparison tests: Aerospace Information Report AIR5666[R]. USA: SAE Aerospace, 2012.
- [16] HINTON G E, SALAKHUTDINOV R R. Reducing the dimensionality of data with neural networks[J]. *Science*, 2006, 313(5786): 504-507.
- [17] HINTON G E. Training products of experts by minimizing contrastive divergence[J]. *Neural Computation*, 2002, 14(8): 1771-1800.
- [18] ZHOU Z H, YI X, GUO L, et al. Quantitative method for ice accretions comparison[J]. *Acta Aerodynamica Sinica*, 2016, 34(5): 556-561.
- [19] WRIGHT W B, RUTKOWSKI A. Validation results for LEWICE 2.0: NASA CR—1999-208690 [R]. USA: NASA, 1999.

Acknowledgements This work was supported in part by the National Natural Science Foundation of China (No. 51606213) and the National Major Science and Technology

Projects (No.J2019-III-0010-0054).

Authors Prof. YI Xian received the B.S. degree from National University of Defense Technology and Ph.D. degree from China Aerodynamics Research and Development Center (CARD). He is the director of Key Laboratory of Icing and Anti-icing of CARD. His research interests include icing numerical computation, icing wind tunnel experimental technology and ice detection technology, etc.

Dr. WANG Qiang received his B.S. degree in Thermal Science and Energy Engineering from University of Science and Technology of China in 2009 and Ph.D. degree in Engineering thermophysics from University of Chinese Academy of

Sciences in 2014. His research interests include icing numerical computation, anti/de-icing technology and application of artificial intelligence in icing analysis, etc.

Author contributions Prof. YI Xian designed the study and conducted the analysis. Dr. WANG Qiang interpreted the results and wrote the manuscript. Miss CHAI Congcong contributed to data and model components for the DNN model. Dr. GUO Lei contributed to the discussion and background of the study. All authors commented on the manuscript draft and approved the submission.

Competing interests The authors declare no competing interests.

(Production Editor: ZHANG Huangqun)

基于深度神经网络的飞机结冰冰形预测模型

易 贤^{1,2,3}, 王 强^{1,2,3}, 柴聪聪^{1,4}, 郭 磊⁴

(1. 中国空气动力研究与发展中心低速空气动力研究所, 绵阳 610082, 中国; 2. 中国空气动力研究与发展中心结冰与防除冰重点实验室, 绵阳 610082, 中国; 3. 空气动力学国家重点实验室, 绵阳 610082, 中国; 4. 电子科技大学计算机科学与工程学院, 成都 610000, 中国)

摘要: 结冰是威胁航空飞行安全的重要因素, 适航条例要求需要根据不同结冰工况开展结冰安全评估。由于飞机结冰过程十分复杂, 快速预测结冰冰形仍是当前面临的重要挑战。基于深度置信神经网络(Deep belief network, DBN)及栈式自动编码器(Stacked auto-encoder, SAE)深度神经网络建立了一种高效的飞机结冰预测模型。在完成网络结构详细设计的基础上, 利用结冰数值计算方法构建的冰形样本空间, 实现神经网络训练。以NACA0012翼型为研究对象, 开展了冰形预测研究。结果表明: 构建的预测模型能够准确地捕捉飞机结冰过程中的非线性行为, 进而实现冰形的高准确度预测。预测模型为飞机结冰分析提供了一种有效的方法。

关键词: 飞机结冰; 冰形预测; 深度神经网络; 深度置信网络; 栈式自动编码器